communications earth & environment

Article

https://doi.org/10.1038/s43247-024-01474-9

Low mercury concentrations in a Greenland glacial fjord attributed to oceanic sources

M. R. Lindeman [1,2] ✉, F. Straneo [1], H. M. Adams [1], M. J. S. Nelson [1] & A. T. Schartup[1]

As the role of the Greenland Ice Sheet in the Arctic mercury (Hg) budget draws scrutiny, it is crucial to understand mercury cycling in glacial fjords, which control exchanges with the ocean. We present full water column measurements of total mercury (THg) and methylmercury (MeHg) in Sermilik Fjord, a large fjord in southeast Greenland fed by multiple marine-terminating glaciers, whose circulation and water mass transformations have been extensively studied. We show that THg (0.23-1.1 pM) and MeHg (0.02-0.17 pM) concentrations are similar to those in nearby coastal waters, while the exported glacially-modified waters are relatively depleted in inorganic mercury (Hg(II)), suggesting that inflowing ocean waters from the continental shelf are the dominant source of mercury species to the fjord. We propose that sediments initially suspended in glacier meltwaters scavenge particle-reactive Hg(II) and are subsequently buried, making the fjord a net sink of oceanic mercury.

The role of the Greenland Ice Sheet in the Arctic mercury (Hg) budget has recently come under scrutiny as a number of studies have investigated Hg concentrations in glacial melt streams[1–5]. Glacial meltwaters transport macronutrients, carbon, and trace elements originating in the ice and subglacial sediments, with significant implications for ocean biogeochemistry[6–8]. In some major Greenland fjords, however, these impacts are secondary to the upwelling of nutrient- and carbon-rich deep ocean waters driven by the release of runoff at the bases of marine-terminating glaciers[9,10]. The vigorous mixing and high particle concentrations in outflowing meltwater plumes may also facilitate removal of exported trace metals (e.g., iron[11,12]). The influence of the Greenland Ice Sheet on downstream Hg distribution therefore depends on its cycling in glacial fjords, which has yet to be specifically studied.

The trace metal Hg is found naturally in the ocean, predominantly in the forms of inorganic divalent mercury (Hg(II)), organic methyl- and dimethyl mercury (together, MeHg), and elemental mercury (Hg(0))[13,14]. However, anthropogenic emissions of Hg have increased globally over the past 150 years, resulting in increased Hg in the atmosphere and ocean[15,16]. Phytoplankton and other primary producers preferentially take up MeHg, a neurotoxicant, which bioaccumulates and biomagnifies in marine food webs and can reach concentrations dangerous to human and ecosystem health at higher trophic levels[17–19]. Indeed, elevated environmental MeHg levels have been found in Arctic food webs, which are central to the diets of many Indigenous communities[20–24].

Many of Greenland's large glacial fjords support productive marine ecosystems that local communities depend upon for their livelihood[9,25–27]. Marine-terminating glaciers such as Helheim Glacier in southeast Greenland, one of Greenland's largest and fastest moving glaciers, have a profound influence on the circulation, water mass properties, and biogeochemistry of the fjords where they terminate[10,28]. Subglacial runoff, formed from surface meltwater that drains to the ice sheet base, carries dissolved and particulate trace elements, potentially including Hg, from the bedrock through subglacial channels and into Sermilik Fjord at Helheim's 600 m-deep grounding line[8,29,30]. This discharge of fresh meltwater at depth forms a buoyant plume, which drives upwelling of macronutrient-rich deep ocean waters and distributes these glacially-modified waters over approximately the upper 200 m of the water column[9,10,31,32]. Water mass transformations in glacial fjords and the influence of non-conservative processes on ocean Hg concentrations, particularly in estuarine and coastal systems, make it challenging to establish the fate of Hg in the coastal waters around Greenland[33–36].

We investigate the role of marine-terminating glaciers and fjord processes in the Greenland Hg cycle by measuring Hg concentrations in Sermilik Fjord (Fig. 1). Using a water mass analysis based on temperature, salinity and dissolved oxygen, we show that the Hg observed in subsurface waters in Sermilik Fjord is imported from the continental shelf. Inside the fjord, we propose that glacial sediments, which are transported by subglacial runoff and icebergs, play an important role in scavenging and burial of Hg(II), which has a high particle affinity[37,38]. Our findings indicate that Sermilik Fjord is a net sink of oceanic Hg(II), and meltwater discharged from this large glacial catchment system is not a measurable source of mercury for the downstream fjord and ocean.

[1]Scripps Institution of Oceanography, University of California San Diego, La Jolla, CA, USA. [2]School of Ocean and Earth Science, National Oceanography Centre, University of Southampton, Southampton, UK. ✉e-mail: margaret.lindeman@gmail.com

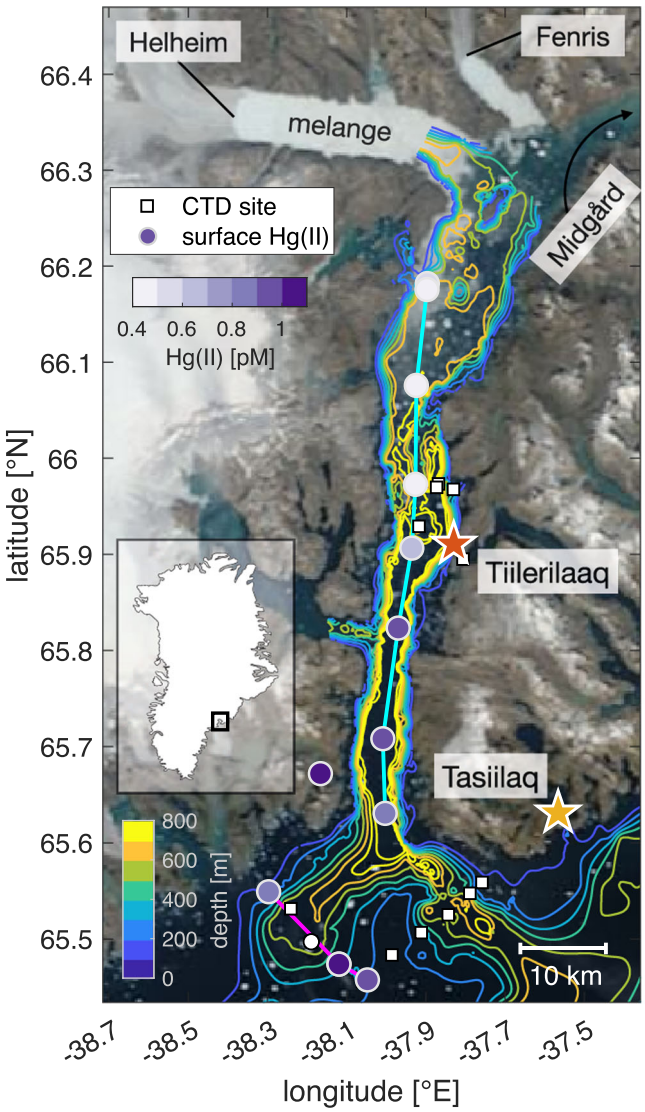

Fig. 1 | Map of Sermilik Fjord region and surface Hg(II) concentrations. MODIS image of Sermilik Fjord and adjacent continental shelf (13 August 2021; NASA Worldview) with inset showing map location within Greenland. The colored circles indicate the surface concentration of inorganic mercury (Hg(II)) where surface samples were taken. At one site on the shelf, only subsurface water samples were collected (small white circle); no water samples were collected at the other CTD sites (white squares). Bathymetry is plotted as colored contours in the fjord and on the continental shelf. The terminus locations of Helheim and Fenris Glaciers are indicated; the terminus of Midgård Glacier is 30 km to the northeast of the field of view. Ice melange, which appears brighter than the grounded ice upstream, extends about 30 km downfjord of Helheim (labeled) and 10 km downfjord of Fenris. The major nearby settlements are Tasiilaq (yellow star) and Tiilerilaaq (formerly Tiniteqilaaq; red star). The west shelf and along-fjord transects shown in Fig. 3 are indicated in magenta and cyan, respectively.

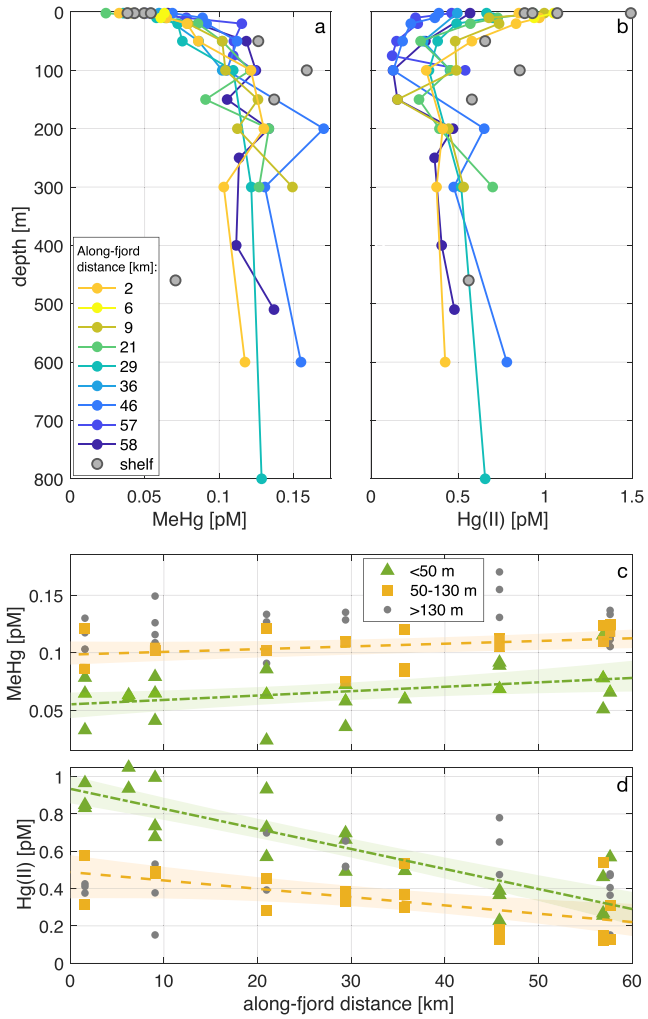

Fig. 2 | Hg concentration profiles and along-fjord trends. Profiles of (**a**) methylmercury (MeHg) and (**b**) inorganic mercury (Hg(II)) concentrations. Fjord profiles are colored by along-fjord distance from the mouth. (The Helheim Glacier terminus is located 90 km from the mouth of the fjord.) Continental shelf samples shown in gray. **c** MeHg and (**d**) Hg(II) concentrations vs. along-fjord distance by density class (green triangles [surface glacially-modified waters (GMW), <50 m], yellow squares [Polar Waters-GMW, 50–130 m], gray circles [>130 m]), with trend line for the upper 100 m (yellow–green dashed line). Shading indicates the 95% confidence interval for best-fit line.

Results

Mercury and water mass distribution in Sermilik Fjord

We find MeHg concentrations of up to 0.17 pM and Hg(II) (defined here as total Hg-MeHg) concentrations of up to 1.0 pM within Sermilik Fjord (Fig. 2a, b). For MeHg, which constitutes 20 ± 11% of total Hg in all samples from Sermilik Fjord, concentrations are lowest in surface waters, ranging between 0.02–0.07 pM in the fjord and 0.04–0.05 pM on the continental shelf, and increasing over the upper 100 m to 0.10–0.15 pM, with little vertical variation deeper in the water column (Fig. 2a). In contrast, the highest overall concentrations of Hg(II) are observed in surface waters (Fig. 2b), and decrease toward the head of the fjord (Fig. 1), with a maximum of 1.0 pM inside the fjord and 1.5 pM on the shelf. Surface water samples were collected from one nearby lake and two rivers fed by smaller land-terminating glaciers disconnected from the ice sheet (Fig. 1, red and yellow stars and Table S1). The freshwater MeHg concentrations ranged from 0.04–0.10 pM and Hg(II) concentrations ranged from 0.69–3.11 pM.

To identify the sources of the Hg detected in the fjord and investigate the potential contribution of glacial meltwater, we first show that Hg concentrations are not elevated in water masses that contain glacial meltwater. The distribution of water masses observed in Sermilik Fjord in summer of 2021 is consistent with that described in earlier surveys of the fjord[31,32,39]. Water masses present at the fjord mouth are similar to those on the continental shelf: fresh, Arctic-sourced Polar Waters (PW; and near-surface Warm Polar Waters) overlying warm, salty Irminger Current-sourced Atlantic Waters (AW) (Figs. 3a and 4; ref. 39). Below 400 m, unmodified AW ($\sigma_0 > 27.5$ kg m^{-3}) is present throughout the fjord (Figs. 3b, c and 4).

Above the AW layer, waters near the head of the fjord have been modified by glacial discharge and glacier melt. Specifically, waters with

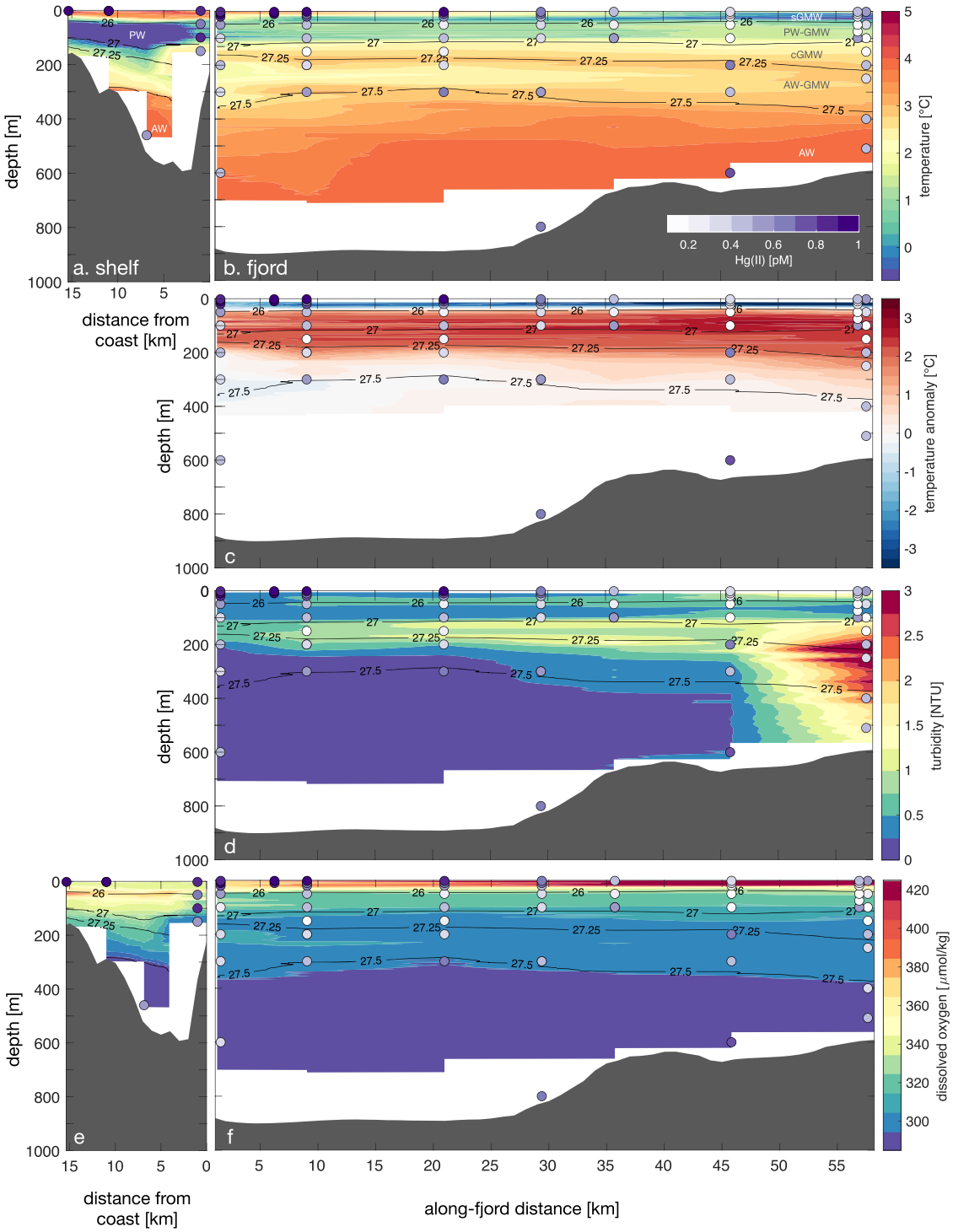

Fig. 3 | Shelf and fjord transects of ocean properties and Hg(II) concentrations. **a** Conservative temperature section for west shelf transect (Fig. 1, magenta). **b** Along-fjord Conservative Temperature section (Fig. 1, cyan). **c** Along-fjord isopycnal temperature anomaly relative to shelf. **d** Along-fjord turbidity. **e** West shelf dissolved oxygen. **f** Along-fjord dissolved oxygen. Hg(II) concentrations are plotted over each section according to colorbar in (**b**). The σ_0 = 26, 27, 27.25 and 27.5 kg m^{-3} isopycnals are overlaid on all sections (black contours) (Polar Waters [PW], Atlantic Waters [AW], surface and core glacially-modified waters [GMW], and mixtures of PW- and AW-GMW) are labeled in (**a**, **b**). In fjord sections, the ice melange is toward the right, with the Helheim Glacier terminus located 90 km along-fjord from the mouth (see map in Fig. 1).

27.5 > σ_0 > 26 kg m^{-3} near the glacier are generally warmer than those found on the shelf and characterized by a relatively high turbidity (Figs. 3c, d and 4). Both of these characteristics, which are amplified toward the glacier, are characteristic of glacially modified waters (GMW), a mixture of subglacial runoff due to surface melt that flows through channels at the glacier bed and enters the fjord at the grounding line, and submarine meltwater from ocean-driven melting of glacier termini and icebergs[28,31,32]. The release of subglacial runoff at depth creates a buoyant upwelling plume that entrains AW, resulting in the warm anomaly (dot-dash mixing line in Fig. 4; refs. 40,41). The sediment enrichment of this GMW, due to release of glacial sediment carried by both subglacial runoff and icebergs[31], is indicated by the high turbidity signal between 150–200 m depth (Fig. 3d). This tongue of elevated

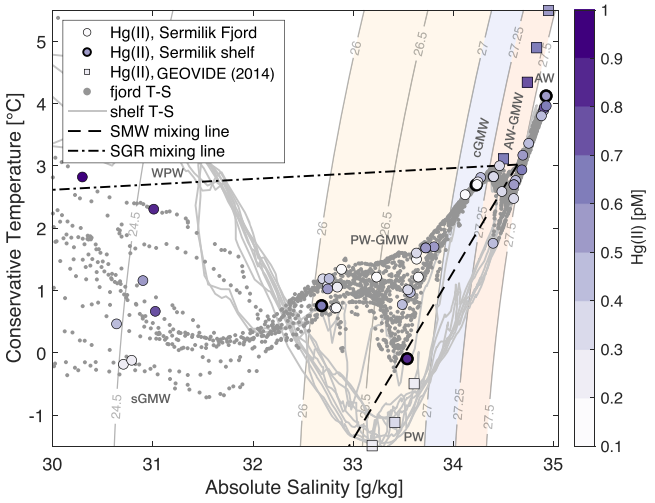

Fig. 4 | Temperature-salinity plot with Hg(II) concentrations. Conservative temperature-absolute salinity plot of Sermilik Fjord (gray dots) and continental shelf (gray lines) with inorganic mercury (Hg(II)) concentration (colored circles; shelf samples have thick black outline). Hg(II) concentrations and corresponding water properties from the 2014 GEOVIDE survey (squares). Mixing lines are plotted for submarine meltwater (SMW; dashed line) and subglacial runoff (SGR; dot-dash line). Shelf water masses Atlantic Waters (AW), Polar Waters (PW), and Warm Polar Waters (WPW) are labeled. Shading is used to highlight density classes highlighted in the text and defined in Table 1. Inside the fjord, these correspond to surface glacially-modified waters (sGMW; unshaded), PW-GMW (yellow), core GMW (blue), AW-GMW (pink), and AW (unshaded), in order of increasing density.

Table 1 | Inorganic mercury (Hg(II)) and methylmercury (MeHg) concentrations in Sermilik Fjord glacially-modified waters (GMW) and Atlantic Waters (AW), and in regional Polar Waters (PW) and AW

Fjord layer[a]	σ_0 [kg m^{-3}]	Depth[b] [m]	Hg(II)[c] [pM]	MeHg[c] [pM]
surface (*n* = 9)	<23	≤2	0.71 ± 0.25	0.05 ± 0.02*
surface GMW (*n* = 22)	<26	<50	0.64 ± 0.25	0.07 ± 0.02*
PW-GMW (*n* = 11)	26–27	50–130	0.34 ± 0.15*	0.11 ± 0.02*
core GMW (*n* = 4)	27–27.25	130–200	0.26 ± 0.15*	0.11 ± 0.02
AW-GMW (*n* = 11)	27.25–27.5	200–350	0.47 ± 0.09	0.13 ± 0.02
AW (*n* = 7)	>27.5	>350	0.57 ± 0.15	0.13 ± 0.02
PW[d] (*n* = 5)	26–27	–	0.29 ± 0.02*	0.12 ± 0.01
AW[d] (*n* = 6)	>27.25	–	0.62 ± 0.07	0.08 ± 0.01

* = significantly different to concentration in fjord AW (95% confidence; *p* values from two-sided *t*-test given in text).
[a]See density class layer definitions in the "Mercury and water mass distribution in Sermilik Fjord" section.
[b]Approximate depth ranges (see Fig. 3).
[c]Hg(II) and MeHg concentrations reported as mean ± standard deviation.
[d]Hg concentrations on Cape Farewell shelf from GEOVIDE 2014[53,77].

turbidity extends along the length of the fjord, and is consistent with the depth of GMW export found in previous studies[42]. This core layer of GMW export is characterized by relatively uniform properties in T-S space (Fig. 4, blue shading).

Above and below the core GMW, along-fjord gradients in temperature and turbidity indicate along-isopycnal mixing between GMW and unmodified shelf waters (Figs. 3b–d and 4; refs. 32,42). These layers are described in Table 1 as PW-GMW and AW-GMW, respectively.

A second, surface-constrained glacially modified water mass (surface GMW) can be identified above 50 m ($\sigma_0 > 26$ kg m^{-3}) as a strongly cooled, relatively high turbidity layer (Fig. 3b–d; ref. 31). Observed temperatures in this layer are below 0 °C in some locations, indicating substantial submarine meltwater input from iceberg melt, in addition to inputs of surface runoff. This layer is also characterized by strong along-fjord gradients toward more shelf-like conditions.

We find that the upper 130 m of the water column (the surface GMW and PW-GMW layers) are significantly lower in MeHg than AW ($p = 10^{-7}$ and $p = 0.004$, respectively), and the core GMW and AW-GMW layers have the same MeHg concentration as AW (Fig. 5b and Table 1). The lack of MeHg enrichment and absence of significant along-fjord trends in the glacially-modified layers (surface GMW: $y = 4{*}10^{-4}x + 0.06$, $R^2 = 0.14$, $p = 0.09$; PW-GMW: $y = 2{*}10^{-4}x + 0.10$, $R^2 = 0.10$, $p = 0.2$; Fig. 2c) suggests that there is no significant MeHg input from meltwater. In general, the magnitude and vertical structure of MeHg concentrations measured at the fjord mouth are consistent with profiles from the Northeast Greenland continental shelf and the Arctic Ocean[43–46].

We find that the fjord-mean Hg(II) profile has a subsurface minimum between 50–200 m, corresponding to the PW-GMW and core GMW layers, which are significantly depleted in Hg(II) compared to AW ($p = 0.004$ and $p = 0.01$, respectively; Fig. 5c and Table 1). There is a strong along-fjord Hg(II) gradient in the surface GMW layer (above 50 m), with highest values near the mouth ($y = -0.011x + 0.935$, $R^2 = 0.74$, $p = 10^{-7}$; Fig. 2d). Similarly, surface Hg(II) concentration (above 2 m) is negatively correlated with along-fjord distance ($y = -0.010x + 1.005$, $R^2 = 0.74$, $p = 0.003$; Fig. 1), and positively correlated with surface salinity, which is highest near the mouth ($y = 0.068x - 0.905$, $R^2 = 0.52$, $p = 0.006$; Fig. S1). The PW-GMW (50–130 m) layer has a weaker but still significant along-fjord trend ($y = -0.005x + 0.488$, $R^2 = 0.33$, $p = 0.01$), while there is no along-fjord trend in the three lower layers. The apparent depletion of Hg(II) in GMW layers and significant along-fjord trends showing that Hg(II) is lowest near the glacier and highest toward the mouth suggest that ocean waters are the primary source of Hg(II) to the fjord.

Water mass mixing model

We use a water mass mixing model based on temperature, salinity and dissolved oxygen to quantify the fraction of each of four water masses (AW, PW, subglacial runoff, submarine meltwater) observed in the fjord. Similar mixing models have been used in Sermilik Fjord, and other glacial fjords in Greenland, using temperature and salinity measurements complemented by noble gas measurements[32,47] or by assuming that the mixing ratio is constant in time, allowing fjord surveys from multiple years to be utilized[48]. Here we instead rely on continuous dissolved oxygen measurements collected together with temperature and salinity profiles within the fjord ("Data collection in Sermilik Fjord" section). This approach utilizes the fact that submarine meltwater is typically supersaturated in dissolved oxygen ("Water mass analysis" section; refs. 49,50) and that the PW and AW originating from the East Greenland Shelf are characterized by distinct dissolved oxygen values[51,52]. On the shelf, PW is generally high in dissolved oxygen, with the highest concentrations (380–400 μmol kg^{-1}) in the near-surface Warm PW layer ($\sigma_0 = 26$ kg m^{-3}), dropping to about 355 μmol kg^{-1} in the PW core (Figs. 3e and S2a and Table 2). AW is characterized by low dissolved oxygen concentration (280 μmol kg^{-1}). The observed dissolved oxygen saturation is around 96–98% in the PW, compared to 88–90% in the AW (Fig. S2a).

In the fjord, dissolved oxygen values in the AW found at depth are similar to values on the shelf, while dissolved oxygen values in the 50–200 m layer are depleted with respect to shelf values (Fig. 3f). This depletion mirrors the fjord temperature anomaly (Fig. 3c), consistent with the upwelling of AW due to mixing with subglacial runoff. Above the core GMW (50–100 m), dissolved oxygen increases toward the shelf due to mixing with PW (Figs. 3f and S2a). The highest dissolved oxygen concentrations are found in very cold, high turbidity waters toward the head of

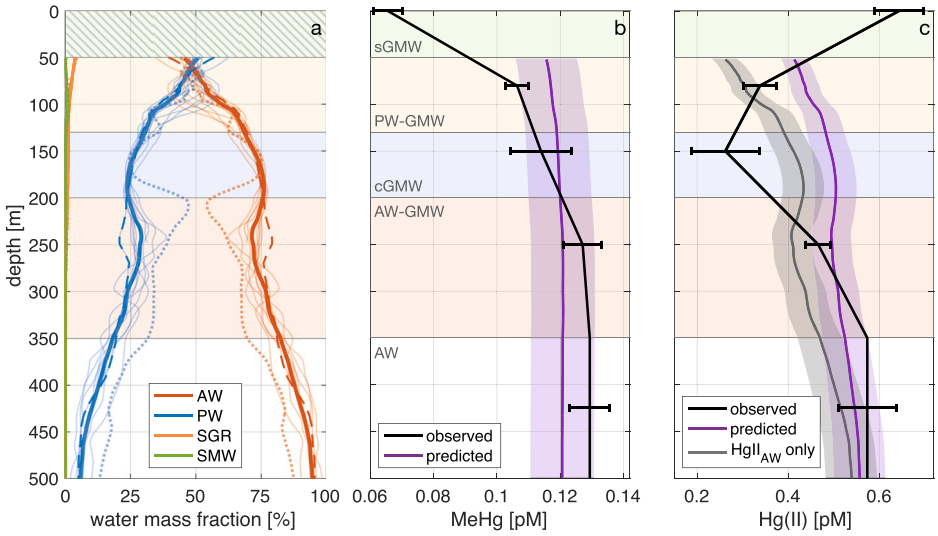

Fig. 5 | Model estimates of water mass concentrations and resulting Hg profiles. a Profiles of estimated concentration of each endmember water mass: Atlantic Waters (AW; red), Polar Waters (PW; blue), subglacial runoff (SGR; orange), and submarine meltwater (SMW; green). Thick solid lines are the fjord mean, with the closest profile to the fjord head indicated by dashed lines and closest to the mouth indicated by dotted lines. Fjord-mean (**b**) methylmercury (MeHg) and (**c**) inorganic mercury (Hg(II)) profile by water mass layer (black; error bars are standard error). Mixing model prediction of mean profiles (purple; shaded uncertainty calculated from error of endmember MeHg concentrations). In (**c**), the AW-only prediction for Hg(II) concentration (gray). The background shading denotes the approximate depth ranges of the fjord density class layers defined in Table 1: surface glacially-modified waters (sGMW; green), PW-GMW (yellow), core GMW (blue), AW-GMW (pink), and AW (unshaded).

Table 2 | Endmember values for conservative temperature (θ), absolute salinity (SA), and dissolved oxygen (DO) concentration used in water mass mixing analysis

Endmember	θ [°C]	SA [g kg^{-1}]	DO [μmol kg^{-1}]
Atlantic Waters	4.0	34.9	280
Polar Waters	−1.5	33.3	355
subglacial runoff	0	0	457
submarine meltwater	−87	0	1050

the fjord. These concentrations are substantially greater than the equilibrium saturation concentration, exceeding 125% at the two northernmost stations and decreasing toward the fjord mouth (Fig. S2b). The spatial distribution of dissolved oxygen in the fjord thus qualitatively supports its application as a tracer of fjord water masses.

Using these observed properties of the two ocean endmembers and published estimates of characteristic subglacial runoff and submarine meltwater properties (Table 2), we decompose each fjord profile into its constituent water masses (Fig. 5a; see "Water mass analysis" section). We find that on average, fjord waters in the subsurface GMW depth range (50–350 m) are composed of 65–85% AW and 15–30% PW. Subglacial runoff and submarine meltwater reach maximum concentrations of about 1–5% near 50 m depth. Compositional variability among the profiles is lowest within the core GMW layer (130–200 m; blue shading), where along-fjord gradients are small. These profiles are similar in both vertical structure and magnitude to a previously-published decomposition of Sermilik Fjord water masses using noble gas tracers[32].

Mixing model predictions of mercury distribution

Since the Hg concentrations of the subglacial runoff and submarine meltwater are unknown, we start by assuming that they contain negligible amounts of Hg. We then use the mean profile of fjord water mass composition (Fig. 5a) and the observed AW and PW Hg concentrations (from our Sermilik survey and GEOVIDE, respectively; Table 1) to construct predicted subsurface profiles of MeHg and Hg(II), assuming they are conserved (purple lines in Fig. 5b, c). These profiles are representative of the expected Hg distribution resulting from mixing and transformation of AW and PW by glacial meltwater input and fjord circulation, but without any additional input of Hg from the ice sheet. Thus they are effectively a lower bound estimate, allowing for the possibility of additional Hg being contributed by subglacial runoff and submarine meltwater. The observed subsurface MeHg and Hg(II) concentrations do not exceed the predicted profiles constructed using the mixing model (Fig. 5b, c), indicating that the fjord Hg content can be accounted for by redistribution of ocean-sourced Hg, without any additional Hg input from meltwaters.

The modeled MeHg profile agrees within uncertainty with the observed mean profile (Fig. 5b). This indicates that our observations are consistent with conservative mixing of oceanic MeHg below 50 m depth. This is also true of the modeled Hg(II) profile below 200 m (Fig. 5c).

However, the modeled Hg(II) profile decreases to a minimum of around 0.4 pM at 50 m depth, overestimating the observed concentrations in both the core GMW and PW-GMW layers (Fig. 5c, purple line). To ensure that the prediction is not artificially inflated by the poorly-constrained PW endmember, we calculate the profile resulting purely from dilution of Hg present in upwelled AW (i.e., assuming PW contains no Hg(II)) and find that Hg(II) in core GMW is still significantly overestimated (Fig. 5c, gray line). We conclude that conservative mixing cannot explain the observed depletion of Hg(II) in GMW exported from Sermilik Fjord.

Discussion

Mercury distribution in a major Greenland glacial fjord

We investigated the Hg distribution in a large Greenland glacial fjord characterized by multiple marine terminating glaciers grounded hundreds of meters below sea level. While earlier studies measured Hg concentrations in melt streams and in the surface waters of glacial fjords, to our knowledge this is the first study to quantify full-water column Hg distribution and apply existing knowledge of the fjord circulation to determine its impact on Hg cycling.

Mercury in the East Greenland Current

Our findings suggest that Atlantic Waters (AW) of subtropical origin are the primary source of Hg to Sermilik Fjord. Near Cape Farewell to the southeast (60°N), both Hg(II) and MeHg concentrations in AW (0.62 ± 0.07 pM and 0.08 ± 0.01 pM, respectively[53]) agreed within uncertainty with the values we measured in Sermilik Fjord (66°N; Table 1), consistent with our understanding that the AW entering Sermilik primarily recirculates south of the Denmark Strait via the Irminger Current[39]. In contrast, a substantial proportion of AW northeast of Greenland circulates through the Arctic Ocean, where the upper water column is enriched in Hg[14]. Total Hg concentrations in AW on the northeast Greenland shelf (79°N) were as high as 4.29 pM, averaging 1.58 ± 0.53 pM over the water column[43]. The agreement between Hg concentrations at Sermilik Fjord and Cape Farewell, in contrast to the northeast, supports the hypothesis that Hg exported from the Arctic to the North Atlantic Ocean is lost through mixing, scavenging, and evasion as AW flows southward in the East Greenland Current, particularly in the Denmark Strait[43].

Mercury in glacial meltwaters

We found no evidence that glacial meltwaters or associated sediments constitute a significant source of Hg species to Sermilik Fjord. Our measurements of Hg(II) and MeHg concentrations in the fjord showed no enrichment beyond ambient ocean levels (Table 1 and Fig. 2a, b), and subsurface glacially-modified waters were in fact depleted in Hg(II) (Fig. 5).

Fjord surface waters contain the greatest proportion of freshwater, comprised primarily of iceberg melt, meltwater runoff, and other terrestrial runoff. Approximating a characteristic ocean surface salinity of 30.4 g kg^{-1} and minimum fjord surface salinity of 21.7 g kg^{-1}, we estimate a maximum freshwater content of roughly 30% for Sermilik Fjord surface waters. The maximum surface concentrations of Hg(II) and MeHg in Sermilik are 1.0 pM and 0.07 pM, respectively (Table 1 and Fig. 2a, b), over one order of magnitude lower than the concentrations reported in surface waters of two West Greenland fjords with comparable freshwater content (12–31 pM and 1.6–2.6 pM[4]). Furthermore, Hg decreases with salinity in those fjords[4], which is a typical estuarine Hg trend (e.g., ref. 54), whereas surface Hg(II) concentration in Sermilik Fjord is lowest toward the head of the fjord (Figs. 1 and 2d) and increases with salinity. The reversal of the typical Hg-salinity trend could be explained by the fact that the freshest surface waters in our survey are near the melange edge and thus contain a relatively large fraction of iceberg melt, evidenced by their very low temperature (≤0 °C) and high dissolved oxygen content (Figs. 4 and S2b), and glacier ice itself is estimated to be relatively low in Hg compared to most Arctic rivers[4,23,55]. In contrast, the fjords sampled by Hawkings et al.[4] are fed in part by land-terminating glaciers, so the higher concentration of proglacial river runoff in their surface waters could make them more similar to typical Arctic estuaries.

Finally, though our melt stream samples were limited, the largest freshwater Hg(II) and MeHg concentrations that we measured near Sermilik Fjord were 3.1 pM and 0.17 pM, respectively, in a river south of Tiilerilaaq ("Mercury and water mass distribution in Sermilik Fjord" section; Table S1). This is comparable to the total Hg observed in Kobbefjord River, which drains a small catchment in West Greenland (3.34 pM[2]), and lower than in Zackenberg River in northeast Greenland (29.5 pM[3]). It is also at the low end of total Hg concentrations observed in a number of West Greenland melt streams, in the range of 3.8–27.1 pM per Jørgensen et al.[5], and much lower than the values reported by Hawkings et al.[4] for those systems.

MeHg: conservative mixing in subsurface GMW and depletion in near-surface waters

We show in Fig. 5b that the observed MeHg concentration in subsurface GMW can be explained by conservative mixing of the constituent water masses. In contrast, we find significant depletion of Hg(II) (Fig. 5c), which is the substrate for methylation. This decoupling suggests that MeHg is not produced within these waters during our sampling period.

We also find that MeHg is significantly lower in the upper 100 m than in the AW layer (Table 1 and Fig. 2a). This characteristic profile typically arises from the effects of evasion and photodemethylation on the two distinct species that comprise MeHg. Dimethylmercury is a dissolved gas within the water column and is influenced by air-sea interactions through evasion and diffusion in surface waters[44,56]. In addition, both monomethylmercury and dimethylmercury are subject to photochemical degradation in the euphotic zone[57,58], which has been estimated as the upper 30–50 m of the water column in Sermilik and similar fjords[10].

Hg(II): depletion in GMW and surface enrichment

Nonconservative behavior of Hg(II), as observed in Sermilik Fjord (Fig. 5c), is common in estuaries, where particulate Hg is typically abundant, leading to much more efficient burial than in the open ocean where the dissolved phase is dominant[14,33,59]. However, while earlier studies have shown that estuaries can moderate riverine fluxes of Hg to the ocean[35], our findings suggest that Sermilik Fjord in fact sequesters oceanic Hg, acting as a net Hg sink.

Assuming that Hg(II) is in equilibrium between its dissolved and particulate phase, an influx of low-Hg glacial sediment into ambient ocean waters could promote scavenging of dissolved oceanic Hg(II) onto sinking particles[37,38,60]. In addition to sediment transport from the ice sheet bed by the subglacial runoff plume[61,62], icebergs release sediment (ice-rafted debris) as they melt, resulting in high sedimentation rates over the 30 km of dense ice melange between the glacier terminus and our northernmost survey site (Fig. 1; ref. 63). We speculate that Hg(II) concentrations in both AW and GMW are altered while transiting through the melange, where settling of abundant subglacial sediment and ice-rafted debris accelerate scavenging of Hg(II) from the water column. Because Hg(II) is more particle-reactive than MeHg[35,64], this mechanism is unlikely to directly affect the distribution of MeHg (which appears to mix conservatively in subsurface GMW).

Jackson and Straneo[42] estimate a mean summertime exchange flow in Sermilik characterized by GMW outflow of about 0.04 m s^{-1} between 100 and 200 m, which would result in a residence time of about 8–9 days in a 30 km-long melange. Silt and clay (grain size < 63 μm), which comprise as much as 90% of sediments deposited from both plume outflow and iceberg melt near the edge of the melange[63], settle at velocities of roughly 100–300 m d^{-1} [61], suggesting that the residence time in the melange is sufficient to allow substantial sediment removal from the upper 200 m.

Our observations show much higher turbidity at depth at the site closest to the melange edge, which drops off dramatically over the 10 km separating it from the next profile (Fig. 3d). Similarly, Andresen et al.[63] find that sedimentation rates at a core between our first and second sites exceed rates at cores near the third and fourth sites by a factor of 3. These findings are consistent with the hypothesis that there could be enhanced scavenging and burial of Hg(II) from the core of GMW outflow in the melange region without significant variation along the remainder of the fjord, as we observe.

Surface concentrations of Hg(II) are lowest at the innermost sample sites and are positively correlated with salinity ("Mercury and water mass distribution in Sermilik Fjord" section; Figs. 1 and 2d). This suggests that, like the underlying PW-GMW layer, the surface is depleted in Hg(II) when it reaches the edge of the melange, but once exposed to the atmosphere, the surface concentration increases further due to mixing with saline ocean water and atmospheric deposition (e.g., ref. 65).

Implications for mercury cycling in Greenland fjords

Our results suggest that glacial meltwater discharged into Sermilik Fjord does not contain significant amounts of Hg. Instead, the Hg found in Sermilik Fjord during summer appears to be supplied primarily by inflowing ocean waters, which are upwelled via the subglacial runoff plume present throughout the summer melt season[28]. Winter conditions, when the meltwater injection is limited to submarine meltwater, will likely present a different Hg distribution. Furthermore, the dynamics of Hg methylation and demethylation are also known to vary seasonally[54].

It is tempting to use these results to estimate Hg(II) burial fluxes in Sermilik Fjord and similar systems. If we approximate that 0.2–0.4 pM of Hg(II) is consistently removed from upwelled AW that is exported with GMW throughout the melt season (Table 1), and use model estimates of subglacial runoff input to estimate AW fluxes (see "AW flux estimate" section), we reach an annual Hg(II) burial flux of roughly 0.1–0.2 kmol $year^{-1}$ in Sermilik Fjord. This estimate is on the same order of magnitude as the burial flux calculated for Lake Melville Fjord in Labrador, Canada (0.62 kmol $year^{-1}$ [54]).

However, even if the hypothesized mechanism is generally correct, other assumptions underlying this estimate remain highly uncertain. The seasonality of subglacial runoff and of regional winds affect the fjord circulation strength and thus the residence time of GMW in the melange, as well as the glacial sediment input and dispersion in the fjord[42,61,66]. If scavenging and burial of Hg(II) occurs gradually along the length of the melange, its efficacy may be very sensitive to residence time, whereas if it mainly occurs close to the terminus, this seasonality may have little impact. Likewise, if this process acts to remove Hg(II) from the water column over relatively long distances and/or residence times, it may be most relevant in

similar systems such as Ilulissat Icefjord, which also has extensive melange[67], whereas if it occurs rapidly in the vicinity of the terminus, it may play a significant role in a broader range of Greenland fjords. Ideally, measurements of Hg concentrations within the melange region could be used to evaluate this mechanism and establish its relevant spatial and temporal scales, but collecting such samples in Sermilik and similar melange-impacted fjords is likely prohibitively difficult. However, characterizing the along-fjord variation in both dissolved and particulate Hg(II) downstream of marine-terminating glaciers without extensive melange would also be useful in addressing some of these questions.

Ultimately, ice sheet meltwater determines the Hg distribution in Sermilik Fjord, not through direct inputs but due to the interaction of the glacier-driven circulation and water mass transformations with Hg-sediment dynamics. A more complete survey of Hg concentrations in ocean waters on the continental shelf around Greenland, as well as in meltwater from glaciers in different regions, is needed to fully understand the role of glacial fjords in Hg cycling.

Methods

Study area

Sermilik Fjord is a large glacial fjord system in southeast Greenland, where Helheim, Fenris and Midgård Glaciers discharge[68]. The grounding lines of Helheim and Fenris Glaciers are 630 m and 380 m below sea level, respectively[69]. The combined catchment area of these three glaciers is about 58,000 km^2, over a third of the southeast GrIS sector[70,71].

Data collection in Sermilik Fjord

Hydrographic data and water samples were collected in Sermilik Fjord and the adjacent shelf region from the M/V Adolf Jensen from August 12–18, 2021[72,73]. Salinity, temperature, and dissolved oxygen profiles were collected using a Seabird 25plus CTD equipped with an SBE 43 dissolved oxygen sensor, which is integrated in the CTD's pumped flow path. All sensors were calibrated prior to shipment to the fjord. A total of 15 profiles were occupied along the length of the fjord and across the fjord inflow and outflow (Fig. 1).

A RBR Concerto CTD system was also mounted as a second, backup system. It carried a complementary Seapoint turbidity sensor that operated in autorange mode (accuracy ± 2% up to 1250 FTU). Temperature, salinity, oxygen, and pressure data are from the Seabird CTD. The complementary turbidity profile, reflecting the amount of suspended sediment present, was obtained from the RBR CTD by projecting turbidity values into pressure bins after cross calibration of the RBR and Seabird pressure sensors. No bottle samples were collected to calibrate the oxygen or turbidity sensors, hence values reported here are interpreted qualitatively and should not be compared directly to other studies. (However, we note that the dissolved oxygen values fall within the range of previous observations on the East Greenland shelf[51,52].).

Mercury sampling

The CTDs were mounted on a rosette carrying eight 8-L bottles (Standard Model 110A, 8 L) fired by a Seabird Autofiring Module at pre-determined depths due to deployment with a non-conductive cable. Inside the fjord, mercury samples were typically taken at 600, 300, 200, 100, 50, 20, 10, and 2 m depth. Outside the fjord, the rosette could not be used due to the sea state. Instead, water samples were collected with two line-mounted Niskin bottles (Model 1010 Niskin Water Sampler, 2.5 L), which limited the number of samples on the shelf.

Surface water samples were also collected by hand at 3 terrestrial sites: one lake and one river near Tiilerilaaq (Fig. 1, red star), and one river near Tasiilaq (Fig. 1, yellow star). These water bodies are fed by glacier melt from smaller ice caps separate from the ice sheet (as well as precipitation).

Samples were collected in 0.25 L precleaned borosilicate glass bottles (I-Chem) for total mercury (THg) and methylmercury (MeHg) analysis. For the cleaning process, all bottles were thoroughly rinsed with ultrapure water (Milli-Q, 18.2 MΩ cm^{-1}). THg bottles were heated to 450 °C in a muffle furnace (Thermo Fisher Scientific), subsequently filled with 1% bromine monochloride, and allowed to sit for at least 3 days. Bottles were then emptied and stored until sampling. MeHg bottles were heated to 450 °C in a muffle furnace (Thermo Fisher Scientific) and stored doubled bagged prior to sampling. After sample collection, both THg and MeHg samples were acidified to 0.4% ultrapure hydrochloric acid (Optima, Fisher Chemical), stored double bagged at 4 °C and analyzed within 6 months of sampling in the Schartup Lab at Scripps Institution of Oceanography.

Total mercury analysis

THg samples were prepared and analyzed following US EPA Method 1631[74]. All Hg species were oxidized to inorganic Hg(II) overnight with bromine monochloride, and then reduced to elemental mercury (Hg(0)) with 20% wt:vol tin(II) chloride solution (J.T. Baker) in 10% hydrochloric acid (Optima, Fisher Chemical). Hg(0) was purged onto a gold trap with Hg-free argon gas and thermally desorbed into a cold-vapor atomic fluorescence spectrometer (CV-AFS) for detection using a Tekran 2600 Automated Mercury Analyzer. Sample concentrations were determined by a calibration curve based on standards prepared from a certified 1000 ppm Hg(II) standard (SPEX CertiPrep). The average THg reagent blank concentration was 0.065 pM (n = 13), the method detection limit (calculated as 3 times the standard deviation of reagent blanks) was 0.23 pM, and ongoing precision and recovery was 100.4 ± 8.2% (n = 11).

Since Hg samples are susceptible to contamination, we transported 2 sample bottles filled with Milli-Q water from the Schartup Lab. These field blanks were acidified during the cruise, stored, and analyzed like the samples. Field blank THg concentrations were 0.08 pM and 0.17 pM, similar to the field blank values in Jørgensen et al.[5]. The field blank values are not deducted from the reported concentrations.

Methyl mercury analysis

MeHg samples were prepared and analyzed by ascorbic acid-assisted direct ethylation following Munson et al.[75] and US EPA Method 1630[76]. Samples were digested overnight with 1% trace metal grade sulfuric acid (Fisher). Samples were then adjusted to a pH of 4.7 using a 2 M acetate/glacial acetic acid buffer (J.T. Baker) in ultrapure water (Milli-Q, 18.2 MW cm^{-1}) and 8 M potassium hydroxide (J.T. Baker) in ultrapure water. In total, 2.5% wt:vol ascorbic acid solution (J.T. Baker) in ultrapure water was added to the samples, then samples were ethylated with sodium tetraethylborate solution (1% NaTEB in 2% potassium hydroxide, Strem) to convert MeHg to volatile methylethylmercury. Ethylation was allowed to proceed for 10 min before sample analysis. Samples were analyzed on a Tekran 2700 Automated Methylmercury Analyzer. Sample concentrations were determined by a calibration curve based on standards prepared from a certified 1000 ppm methylmercury(II) chloride standard (Alfa Aesar). For MeHg, reagent blank peaks are often too small to be calculated, but the average of the detectable peaks is 0.003 pM (n = 10), the method detection limit was 0.0156 pM, and ongoing precision and recovery was 102.9 ± 2.7% (n = 15).

The Hg(II) concentrations presented are calculated as the residual of THg and MeHg, so these values also include any Hg(0) converted to Hg(II) by acidification.

GEOTRACES data

We supplement our limited samples of ocean water masses on the shelf with Hg(II) and MeHg concentrations from the 2014 GEOVIDE survey[77]. These samples were collected during June 2014 at Stations 53 and 56, which are located on the continental shelf east of Cape Farewell, approximately 700 km SSW of Sermilik Fjord[53]. The use of these values is supported by the close overlap of the water mass properties in T-S space with the 2021 observations on the continental shelf (Fig. 4) and the similarity in AW mercury concentrations (Table 1).

Water mass analysis

Based on previous studies (e.g., refs. 31,32,42,78), we expect that the majority of waters in Sermilik Fjord are constituted from mixing of four

endmembers: the two shelf water masses, Atlantic Waters (AW) and Polar Waters (PW), and the two glacial inputs, submarine meltwater (SMW) and subglacial runoff (SGR) (Fig. 4). Near the surface we expect the ocean properties to also be influenced by mixing with Warm Polar Waters and nonconservative surface processes (e.g., insolation, air-sea fluxes, primary production); therefore we exclude the upper 50 m from this analysis.

SGR is represented on the T-S plot as a water mass with zero salinity and temperature at the local freezing point (~0 °C), which mixes with the ambient ocean properties at the grounding line depth (Fig. 4, dot-dash line). To represent SMW, the combined effects of latent heat uptake and meltwater input are represented by mixing with freshwater at an "effective temperature" of ~ − 87 °C (Fig. 4, dashed line[28,79]).

In addition to interpretation of the T-S plot, we quantitatively decompose the fractions of the four major endmembers in our observations using a simple linear mixing model[80]. The properties resulting from conservative mixing between n water masses can be represented as a linear system of equations:

$$\mathbf{Ax} - \mathbf{d} = \mathbf{r}, \tag{1}$$

where $\mathbf{A}$ is the $n \times n$ matrix of constraints ($n - 1$ endmember tracer values, and mass conservation), $\mathbf{x}$ is the unknown $n \times 1$ vector of water mass fractions, $\mathbf{d}$ is the $n \times 1$ vector of observed tracer values, and $\mathbf{r}$ is the $n \times 1$ residual misfit. We calculate the least squares solution of $\mathbf{x}$ for each observation, requiring that all water mass fraction values must be greater than or equal to 0.

We use dissolved oxygen as an independent constraint for the decomposition, in addition to temperature and salinity. Dissolved oxygen has been used for similar analyses in the Amundsen Sea, where there are three major endmembers (two ocean water masses and SMW[50,81,82]). As in those studies, we exclude the near-surface ocean from the analysis to eliminate the influence of air-sea fluxes, and approximate that subsurface dissolved oxygen is a conservative tracer over the depth range and time scale relevant to this study.

The endmember tracer values used in our analysis are given in Table 2. We estimate AW and PW temperature, salinity, and dissolved oxygen concentrations from CTD profiles measured on the shelf ("Mercury and water mass distribution in Sermilik Fjord" section; Figs. 3e, 4, and S2). For the glacial inputs, we use the established characteristic temperature and salinity and estimate dissolved oxygen concentrations following Beaird et al.[47]. SMW is formed by glacial ice melting beneath the ocean surface, so we calculate the resulting oxygen concentration assuming that all gases contained in the ice are forced into solution[47,49,83]. In contrast, SGR originates as surface melt, so we calculate the saturation concentration of 0°C freshwater at atmospheric pressure, assuming that the meltwater is at the surface long enough to equilibrate with the atmosphere[47].

The SMW and SGR dissolved oxygen concentrations are relatively uncertain compared to the other endmember tracer values. Our analysis primarily focuses on large vertical variations in the AW and PW concentrations, and our key result is not sensitive to this uncertainty. However, more careful sensitivity analysis would be needed to precisely quantify small concentrations of meltwater in Sermilik Fjord using this method.

We apply the model presented in the "Water mass mixing model" section to determine whether the observed mercury concentrations in glacially modified waters are consistent with conservative mixing. According to our mixing model, the observed concentration of a conserved tracer, χ_{obs}, can be represented by:

$$\chi_{obs} = a * \chi_{AW} + b * \chi_{PW} + c * \chi_{SGR} + d * \chi_{SMW}, \tag{2}$$

where χ_i is the tracer concentration in endmember i, and a, b, c, and d are the fractions of the corresponding endmember in the observed water parcel. In this case, χ_{SGR} and χ_{SMW} are set to zero to calculate the purple profiles in Fig. 5b, c, as explained in the "Mixing model predictions of mercury distribution" section, and χ_{PW} is additionally set to zero to calculate the gray profile in Fig. 5c.

AW flux estimate

We calculate the mean annual SGR input to Sermilik Fjord from Helheim and Fenris Glaciers using the dataset of Mankoff et al.[84]. Following Cape et al.[10], the associated AW upwelling flux is calculated, applying 3 values of the entrainment ratio $\frac{f_{AW}}{f_{SGR}}$ ranging from 30–80 based on published estimates[10,32,69]. This value is then converted to Hg(II) flux by approximating that the Hg(II) concentration of inflowing AW is constant, and that a constant proportion of Hg(II) ranging from 0.2–0.4 pM is removed from upwelled AW that is exported with GMW throughout the melt season.

Reporting summary

Further information on research design is available in the Nature Portfolio Reporting Summary linked to this article.

Data availability

All data collected for this study in Sermilik Fjord during August 2021 are publicly available via the NSF Arctic Data Center (CTD data: https://doi.org/10.18739/A2HD7NT9K) and Zenodo (Hg data: https://doi.org/10.5281/zenodo.7890489).

Received: 23 August 2023; Accepted: 30 May 2024;
Published online: 13 June 2024

References

1. Rigét, F. et al. Mercury (Hg) transport in a high Arctic River in Northeast Greenland. *Water Air Soil Pollut.* **222**, 233–242 (2011).
2. Søndergaard, J., Rigét, F., Tamstorf, M. P. & Larsen, M. M. Mercury transport in a low-Arctic river in Kobbefjord, West Greenland (64° N). *Water Air Soil Pollut*. **223**, 4333–4342 (2012).
3. Søndergaard, J. et al. Mercury exports from a high-Arctic river basin in Northeast Greenland (74°N) largely controlled by glacial lake outburst floods. *Sci. Total Environ.* **514**, 83–91 (2015).
4. Hawkings, J. R. et al. Large subglacial source of mercury from the southwestern margin of the Greenland Ice Sheet. *Nat. Geosci.* **14**, 496–502 (2021).
5. Jørgensen, C. J. et al. Large mercury release from the Greenland Ice Sheet invalidated. *Sci. Adv.* **10**, eadi7760 (2024).
6. Bhatia, M. P. et al. Greenland meltwater as a significant and potentially bioavailable source of iron to the ocean. *Nat. Geosci.* **6**, 274–278 (2013).
7. Wadham, J. L. et al. Ice sheets matter for the global carbon cycle. *Nat. Commun.* **10**, 3567 (2019).
8. Hawkings, J. R. et al. Enhanced trace element mobilization by Earth's ice sheets. *Proc. Natl Acad. Sci.* **117**, 31648–31659 (2020).
9. Meire, L. et al. Marine-terminating glaciers sustain high productivity in Greenland fjords. *Glob. Change Biol.* **23**, 5344–5357 (2017).
10. Cape, M. R., Straneo, F., Beaird, N., Bundy, R. M. & Charette, M. A. Nutrient release to oceans from buoyancy-driven upwelling at Greenland tidewater glaciers. *Nat. Geosci.* **12**, 34–39 (2019).
11. Hopwood, M. J. et al. Seasonal changes in Fe along a glaciated Greenlandic fjord. *Front. Earth Sci.* **4**, 15 (2016).
12. Kanna, N., Sugiyama, S., Fukamachi, Y., Nomura, D. & Nishioka, J. Iron supply by subglacial discharge into a fjord near the front of a marine-terminating glacier in Northwestern Greenland. *Glob. Biogeochem. Cycles* **34**, e2020GB006567 (2020).
13. Selin, N. E. Global biogeochemical cycling of mercury: a review. *Annu. Rev. Environ. Resour.* **34**, 43–63 (2009).
14. Bowman, K. L., Lamborg, C. H. & Agather, A. M. A global perspective on mercury cycling in the ocean. *Sci. Total Environ.* **710**, 136166 (2020).
15. Amos, H. M., Jacob, D. J., Streets, D. G. & Sunderland, E. M. Legacy impacts of all-time anthropogenic emissions on the global mercury cycle. *Glob. Biogeochem. Cycles* **27**, 410–421 (2013).

16. Lamborg, C. H. et al. A global ocean inventory of anthropogenic mercury based on water column measurements. *Nature* **512**, 65–68 (2014).
17. Pickhardt, P. C. & Fisher, N. S. Accumulation of inorganic and methylmercury by freshwater phytoplankton in two contrasting water bodies. *Environ. Sci. Technol.* **41**, 125–131 (2007).
18. Chen, C. Y. et al. Mercury bioavailability and bioaccumulation in estuarine food webs in the Gulf of Maine. *Environ. Sci. Technol.* **43**, 1804–1810 (2009).
19. Schartup, A. T. et al. A model for methylmercury uptake and trophic transfer by marine plankton. *Environ. Sci. Technol.* **52**, 654–662 (2018).
20. Dewailly, E. et al. Exposure of the Inuit population of Nunavik (Arctic Québec) to lead and mercury. *Arch. Environ. Health* **56**, 350–357 (2001).
21. Lavoie, R. A., Jardine, T. D., Chumchal, M. M., Kidd, K. A. & Campbell, L. M. Biomagnification of mercury in aquatic food webs: a worldwide meta-analysis. *Environ. Sci. Technol.* **47**, 13385–13394 (2013).
22. Stern, G. A. et al. How does climate change influence arctic mercury? *Sci. Total Environ.* **414**, 22–42 (2012).
23. Dastoor, A. et al. Arctic mercury cycling. *Nat. Rev. Earth Environ.* **3**, 270–286 (2022).
24. Basu, N. et al. The impact of mercury contamination on human health in the Arctic: a state of the science review. *Sci. Total Environ.* **831**, 154793 (2022).
25. Nuttall, M. Water, ice, and climate change in northwest Greenland. *WIREs Water* **7**, e1433 (2020).
26. Muntjewerf, L. et al. Greenland Ice Sheet contribution to 21st century sea level rise as simulated by the coupled CESM2.1-CISM2.1. *Geophys. Res. Lett.* **47**, e2019GL086836 (2020).
27. Straneo, F. et al. An interdisciplinary perspective on Greenland's changing coastal margins. *Oceanography* **35**, 106–117 (2022).
28. Straneo, F. & Cenedese, C. The dynamics of Greenland's glacial fjords and their role in climate. *Annu. Rev. Mar. Sci.* **7**, 89–112 (2015).
29. Chu, V. W. Greenland ice sheet hydrology: a review. *Prog. Phys. Geogr. Earth Environ.* **38**, 19–54 (2014).
30. Enderlin, E. M. et al. An improved mass budget for the Greenland ice sheet. *Geophys. Res. Lett.* **41**, 866–872 (2014).
31. Straneo, F. et al. Impact of fjord dynamics and glacial runoff on the circulation near Helheim Glacier. *Nat. Geosci.* **4**, 322–327 (2011).
32. Beaird, N. L., Straneo, F. & Jenkins, W. Export of strongly diluted Greenland meltwater from a major glacial fjord. *Geophys. Res. Lett.* **45**, 4163–4170 (2018).
33. Amos, H. M. et al. Global biogeochemical implications of mercury discharges from rivers and sediment burial. *Environ. Sci. Technol.* **48**, 9514–9522 (2014).
34. Bruland, K. W. & Lohan, M. C. Controls of trace metals in seawater. in *Treatise on Geochemistry*, Vol. 6 (eds Holland, H. D. & Turekian, K. K.) Ch. 2, 23–47 (Elsevier, 2003).
35. Buck, C. S., Hammerschmidt, C. R., Bowman, K. L., Gill, G. A. & Landing, W. M. Flux of total mercury and methylmercury to the northern Gulf of Mexico from U.S. estuaries. *Environ. Sci. Technol.* **49**, 13992–13999 (2015).
36. Krause, J. et al. Trace element (Fe, Co, Ni and Cu) dynamics across the salinity gradient in Arctic and Antarctic glacier fjords. *Front. Earth Sci.* **9**, 725279 (2021).
37. Lamborg, C. H., Hammerschmidt, C. R. & Bowman, K. L. An examination of the role of particles in oceanic mercury cycling. *Philos. Trans. R. Soc. A Math. Phys. Eng. Sci.* **374**, 20150297 (2016).
38. Cui, X., Lamborg, C. H., Hammerschmidt, C. R., Xiang, Y. & Lam, P. J. The effect of particle composition and concentration on the partitioning coefficient for mercury in three ocean basins. *Front. Environ. Chem.* **2**, 660267 (2021).
39. Straneo, F. et al. Characteristics of ocean waters reaching Greenland's glaciers. *Ann. Glaciol.* **53**, 202–210 (2012).
40. Slater, D. A., Goldberg, D. N., Nienow, P. W. & Cowton, T. R. Scalings for submarine melting at tidewater glaciers from buoyant plume theory. *J. Phys. Oceanogr.* **46**, 1839–1855 (2016).
41. Melton, S. M. et al. Meltwater drainage and iceberg calving observed in high-spatiotemporal resolution at Helheim Glacier, Greenland. *J. Glaciol.* **68**, 812–828 (2022).
42. Jackson, R. H. & Straneo, F. Heat, salt, and freshwater budgets for a glacial fjord in Greenland. *J. Phys. Oceanogr.* **46**, 2735–2768 (2016).
43. Petrova, M. V. et al. Mercury species export from the Arctic to the Atlantic Ocean. *Mar. Chem.* **225**, 103855 (2020).
44. Agather, A. M., Bowman, K. L., Lamborg, C. H. & Hammerschmidt, C. R. Distribution of mercury species in the Western Arctic Ocean (U.S. GEOTRACES GN01). *Mar. Chem.* **216**, 103686 (2019).
45. Heimburger, L. E. et al. Shallow methylmercury production in the marginal sea ice zone of the central Arctic Ocean. *Sci. Rep.* **5**, 10318 (2015).
46. Wang, K. et al. Subsurface seawater methylmercury maximum explains biotic mercury concentrations in the Canadian Arctic. *Sci. Rep.* **8**, 14465 (2018).
47. Beaird, N. L., Straneo, F. & Jenkins, W. Spreading of Greenland meltwaters in the ocean revealed by noble gases. *Geophys. Res. Lett.* **42**, 7705–7713 (2015).
48. Muilwijk, M. et al. Export of ice sheet meltwater from Upernavik Fjord, West Greenland. *J. Phys. Oceanogr.* **52**, 363–382 (2022).
49. Hellmer, H. H., Jacobs, S. S. & Jenkins, A. Oceanic erosion of a floating Antarctic glacier in the Amundsen Sea. in *Ocean, Ice, and Atmosphere: Interactions at the Antarctic Continental Margin*, Vol. 75 (eds Jacobs, S. S. & Weiss, R. F.) 83–99 (American Geophysical Union (AGU), 1998).
50. Jenkins, A. The impact of melting ice on ocean waters. *J. Phys. Oceanogr.* **29**, 2370 – 2381 (1999).
51. Pickart, R. S., Torres, D. J. & Fratantoni, P. S. The East Greenland spill jet. *J. Phys. Oceanogr.* **35**, 1037–1053 (2005).
52. García-Ibáñez, M. I. et al. Water mass distributions and transports for the 2014 GEOVIDE cruise in the North Atlantic. *Biogeosciences* **15**, 2075–2090 (2018).
53. Cossa, D. et al. Mercury distribution and transport in the North Atlantic Ocean along the GEOTRACES-GA01 transect. *Biogeosciences* **15**, 2309–2323 (2018).
54. Schartup, A. T. et al. Freshwater discharges drive high levels of methylmercury in Arctic marine biota. *Proc. Natl Acad. Sci. USA* **112**, 11789–11794 (2015).
55. Soerensen, A. L. et al. A mass budget for mercury and methylmercury in the Arctic Ocean. *Glob. Biogeochem. Cycles* **30**, 560–575 (2016).
56. Baya, P. A., Gosselin, M., Lehnherr, I., St.Louis, V. L. & Hintelmann, H. Determination of monomethylmercury and dimethylmercury in the Arctic marine boundary layer. *Environ. Sci. Technol.* **49**, 223–232 (2015).
57. West, J., Gindorf, S. & Jonsson, S. Photochemical degradation of dimethylmercury in natural waters. *Environ. Sci. Technol.* **56**, 5920–5928 (2022).
58. DiMento, B. P. & Mason, R. P. Factors controlling the photochemical degradation of methylmercury in coastal and oceanic waters. *Mar. Chem.* **196**, 116–125 (2017).
59. Choe, K.-Y., Gill, G. A. & Lehman, R. Distribution of particulate, colloidal, and dissolved mercury in San Francisco Bay estuary. 1. Total mercury. *Limnol. Oceanogr.* **48**, 1535–1546 (2003).
60. Morel, F. M. M., Kraepiel, A. M. L. & Amyot, M. The chemical cycle and bioaccumulation of mercury. *Annu. Rev. Ecol. Evol. Syst.* **29**, 543–566 (1998).
61. Mugford, R. I. & Dowdeswell, J. A. Modeling glacial meltwater plume dynamics and sedimentation in high-latitude fjords. *J. Geophys. Res. Earth Surf.* **116**, F01023 (2011).
62. Sutherland, B. R., Rosevear, M. G. & Cenedese, C. Laboratory experiments modeling the transport and deposition of sediments by

glacial plumes rising under an ice shelf. *Phys. Rev. Fluids* **5**, 013802 (2020).
63. Andresen, C. S. et al. Rapid response of Helheim Glacier in Greenland to climate variability over the past century. *Nat. Geosci.* **5**, 37–41 (2012).
64. Lawson, N. M., Mason, R. P. & Laporte, J.-M. The fate and transport of mercury, methylmercury, and other trace metals in Chesapeake Bay tributaries. *Water Res.* **35**, 501–515 (2001).
65. Zhang, Y., Jaeglé, L. & Thompson, L. Natural biogeochemical cycle of mercury in a global three-dimensional ocean tracer model. *Glob. Biogeochem. Cycles* **28**, 553–570 (2014).
66. Jackson, R. H., Straneo, F. & Sutherland, D. A. Externally forced fluctuations in ocean temperature at Greenland glaciers in non-summer months. *Nat. Geosci.* **7**, 503–508 (2014).
67. Kajanto, K., Straneo, F. & Nisancioglu, K. Impact of icebergs on the seasonal submarine melt of Sermeq Kujalleq. *Cryosphere* **17**, 371–390 (2023).
68. Straneo, F., Hamilton, G. S., Stearns, L. A. & Sutherland, D. A. Connecting the Greenland Ice Sheet and the ocean: a case study of Helheim Glacier and Sermilik Fjord. *Oceanography* **29**, 34–45 (2016).
69. Slater, D. A. et al. Characteristic depths, fluxes, and timescales for Greenland's tidewater glacier fjords from subglacial discharge driven upwelling during summer. *Geophys. Res. Lett.* **49**, e2021GL097081 (2022).
70. Mernild, S. H. et al. Freshwater flux to Sermilik Fjord, SE Greenland. *Cryosphere* **4**, 453–465 (2010).
71. Mouginot, J. et al. Forty-six years of Greenland Ice Sheet mass balance from 1972 to 2018. *Proc. Natl Acad. Sci.* **116**, 9239 LP – 9244 (2019).
72. Straneo, F. *Temperature, Salinity, Dissolved Oxygen, and Turbidity Profiles from Sermilik Fjord, East Greenland, Collected Over August 12-18, 2021* (Arctic Data Center, 2023).
73. Lindeman, M. R., Straneo, F., Adams, H. M., Nelson, M. J. S. & Schartup, A. T. Data for: Low mercury concentration in a Greenland glacial fjord attributed to oceanic sources. https://zenodo.org/records/7890489 (2023).
74. US Environmental Protection Agency. Method 1631, revision e: Mercury in water by oxidation, purge and trap, and cold vapor atomic fluorescence spectrometry. https://www.epa.gov/sites/default/files/2015-08/documents/method_1631e_2002.pdf (2002).
75. Munson, K. M., Babi, D. & Lamborg, C. H. Determination of monomethylmercury from seawater with ascorbic acid-assisted direct ethylation. *Limnol. Oceanogr. Methods* **12**, 1–9 (2014).
76. US Environmental Protection Agency. Method 1630, methyl mercury in water by distillation, aqueous ethylation, purge and trap, and cold vapor atomic fluorescence spectrometry. https://www.epa.gov/sites/default/files/2015-08/documents/method_1630_1998.pdf (1998).
77. GEOTRACES Intermediate Data Product Group. The GEOTRACES Intermediate Data Product 2021 (IDP2021). (2021).
78. Straneo, F. et al. Rapid circulation of warm subtropical waters in a major glacial fjord in East Greenland. *Nat. Geosci.* **3**, 182–186 (2010).
79. Gade, H. G. Melting of ice in sea water: a primitive model with application to the Antarctic Ice Shelf and icebergs. *J. Phys. Oceanogr.* **9**, 189–198 (1979).
80. Tomczak, M. A multi-parameter extension of temperature/salinity diagram techniques for the analysis of non-isopycnal mixing. *Prog. Oceanogr.* **10**, 147–171 (1981).
81. Biddle, L. C., Heywood, K. J., Kaiser, J. & Jenkins, A. Glacial meltwater identification in the Amundsen Sea. *J. Phys. Oceanogr.* **47**, 933–954 (2017).
82. Biddle, L. C., Loose, B. & Heywood, K. J. Upper ocean distribution of glacial meltwater in the Amundsen Sea, Antarctica. *J. Geophys. Res. Oceans* **124**, 6854–6870 (2019).
83. Martinerie, P., Raynaud, D., Etheridge, D. M., Barnola, J.-M. & Mazaudier, D. Physical and climatic parameters which influence the air content in polar ice. *Earth Planet. Sci. Lett.* **112**, 1–13 (1992).
84. Mankoff, K. D. et al. Greenland liquid water discharge from 1958 through 2019. *Earth Syst. Sci. Data* **12**, 2811–2841 (2020).

Acknowledgements

The authors gratefully acknowledge the crew of MV Adolf Jensen, based in Qaqortoq, Kalaallit Nunaat (South Greenland). Jamie Holte and Donald Slater assisted with sampling in the field, and Jamie Holte processed and archived the CTD data. Three anonymous reviewers provided valuable feedback on an earlier version of this manuscript. The 2021 Sermilik Fjord field campaign was supported by funding from the Heising Simons Foundation to F.S. and an SIO Seed Fund grant to F.S. and A.T.S. M.R.L. and M.J.S.N. were additionally supported by NSF funding to F.S. A.T.S. received funding from the Alfred P. Sloan Foundation and H.M.S. was supported by US National Science Foundation grant OCE 2023046 to A.T.S. We acknowledge the use of imagery from the NASA Worldview application (https://worldview.earthdata.nasa.gov/), part of the NASA Earth Observing System Data and Information System (EOSDIS). No permissions were needed to collect the water samples analyzed for this study.

Author contributions

F.S. and A.T.S. conceived the study and obtained funding. F.S. led the field campaign and M.J.S.N. and M.R.L. collected samples in the field. H.M.A. and A.T.S. prepared the sampling materials and analyzed samples in the lab. M.R.L. analyzed and interpreted the data with input from F.S., H.M.A., and A.T.S. M.R.L. wrote the manuscript with contributions from H.M.A. and M.J.S.N., and all coauthors provided feedback throughout the writing and revision process.

Competing interests

The authors declare no competing interests.

Additional information

Supplementary information The online version contains supplementary material available at https://doi.org/10.1038/s43247-024-01474-9.

Correspondence and requests for materials should be addressed to M. R. Lindeman.